Yeast Ribonuclease III Uses a Network of Multiple Hydrogen Bonds for RNA Binding and Cleavage[†]

Mathieu Lavoie and Sherif Abou Elela*

Groupe ARN/RNA Group, Département de Microbiologie et d'Infectiologie, Faculté de Médecine et des Sciences de la Santé, Université de Sherbrooke, Sherbrooke, Québec, Canada J1H 5N4

Received February 9, 2008; Revised Manuscript Received June 20, 2008

ABSTRACT: Members of the bacterial RNase III family recognize a variety of short structured RNAs with few common features. It is not clear how this group of enzymes supports high cleavage fidelity while maintaining a broad base of substrates. Here we show that the yeast orthologue of RNase III (Rnt1p) uses a network of 2′-OH-dependent interactions to recognize substrates with different structures. We designed a series of bipartite substrates permitting the distinction between binding and cleavage defects. Each substrate was engineered to carry a single or multiple 2′-*O*-methyl or 2′-fluoro ribonucleotide substitutions to prevent the formation of hydrogen bonds with a specific nucleotide or group of nucleotides. Interestingly, introduction of 2′-*O*-methyl ribonucleotides near the cleavage site increased the rate of catalysis, indicating that 2′-OH are not required for cleavage. Substitution of nucleotides in known Rnt1p binding site with 2′-*O*-methyl ribonucleotides inhibited cleavage while single 2′-fluoro ribonucleotide substitutions did not. This indicates that while no single 2′-OH is essential for Rnt1p cleavage, small changes in the substrate structure are not tolerated. Strikingly, several nucleotide substitutions greatly increased the substrate dissociation constant with little or no effect on the Michaelis−Menten constant or rate of catalysis. Together, the results indicate that Rnt1p uses a network of nucleotide interactions to identify its substrate and support two distinct modes of binding. One mode is primarily mediated by the dsRNA binding domain and leads to the formation of stable RNA/protein complex, while the other requires the presence of the nuclease and N-terminal domains and leads to RNA cleavage.

The bacterial RNase III family is comprised of enzymes that specifically cleave RNA duplexes (*1, 2*) to regulate gene expression (*3*), process noncoding RNA (*4–6*), and enforce cellular immunity (*7*). The RNase III family is divided into four classes, based on protein features (*1*). Class I includes bacterial enzymes that possess a single N-terminal nuclease domain (NUCD)[1] and a C-terminal double-stranded RNA binding domain (dsRBD) (*8*). Class II enzymes, which are found in fungi, possess in addition to the NUCD and the dsRBD a highly variable N-terminal domain with no apparent functional motifs. Class III enzymes contain two NUCDs and include plant and vertebrate enzymes like human Drosha (*9*). Class IV includes the RNAi enzyme Dicer, which possesses N-terminal helicase and PAZ domains (*10*). Yeast Rnt1p (*11*) is a class II enzyme harboring a dsRBD motif followed by a C-terminal extension required for nucleolar localization (*12*). The NUCD of Rnt1p exhibits the RNase III signature sequence implicated in catalysis. Rnt1p's N-terminal extension promotes enzyme homodimerization and is required for efficient cleavage at high salt concentrations (*13*). Recently, crystal (*14*) and solution (*15*) structures of Rnt1p dsRBD confirmed the classical $\alpha\beta\beta\beta\alpha$ structure and revealed an additional helix near the C-terminus ($\alpha3$) that is unique to Rnt1p. The solution structure of the dsRBD/RNA complex (*15*) indicates that the additional helix is not located near the substrate RNA but that it could influence the binding of RNA to $\alpha1$ (*14*).

In bacteria, RNase III discriminates its substrates from other structured RNAs using antideterminant nucleotides, and as such, it is the absence of certain substrate features and not their presence that triggers RNA cleavage (*16*). In contrast, eukaryotic RNase III uses different mechanisms of substrate selectivity in which antideterminants play a minor role (*17*). For example, Rnt1p prefers substrates that exhibit an NGNN (G2) or AAGU (A1) tetraloop structure (*18*). This unique preference for G2 or A1 loops is likely due to differences in the protein structure, such as the additional helix ($\alpha3$) at the end of Rnt1p dsRBD. The structure of the Rnt1p dsRBD/RNA complex (*15*) shows that the protein monomer contacts both the RNA major and minor grooves but, surprisingly, not the conserved G in the second position of the terminal tetraloop (*17*). Deletion of this tetraloop, or substitution of the universally conserved G, inhibits cleavage

[†] This work was supported by a grant from the Canadian Institute for Health Research (CIHR). S.A. is a Chercheur-Boursier Senior of the Fonds de la Recherche en Santé du Québec. M.L. acknowledges support from FQRNT.

* To whom correspondence should be addressed. Phone: (819) 564-5275. Fax: (819) 564-5392. E-mail: Sherif.Abou.Elela@USherbrooke.ca.

[1] Abbreviations: Rnt1p, *Saccharomyces cerevisiae* orthologue of bacterial RNase III; dsRNA, double-stranded RNA; NUCD, nuclease domain; dsRBD, double-stranded RNA binding domain; G2 and A1 loops, RNA stems capped with a NGNN or AAGU tetraloop, respectively; 2′-O-Me, 2′-*O*-methyl ribonucleotide; 2′-F, 2′-fluoro ribonucleotide; TL, target RNA; EMSA, electrophoretic mobility shift assay; dT, inverted deoxythymidine; ΔN-term, recombinant version of Rnt1p lacking the N-terminal extension; RBM, RNA binding motif.

10.1021/bi800238u CCC: $40.75
Published on Web 07/23/2008

and reduces binding under physiological conditions (*19*). To explain the lack of interaction between the dsRBD and the conserved G, it was suggested that this nucleotide does not directly contribute to substrate recognition but instead confers a structural fold recognized by Rnt1p (*20*). However, Rnt1p fails to cleave RNA hairpins capped with an ACAA tetraloop, which have an overall conformation that is similar to G2 loops (*21*) and recognizes the A1 loops that adopt a different structure (*22*). It is not clear how Rnt1p distinguishes between RNAs with seemingly different structures and sequence from others that appear to be structurally similar to known substrates.

The crystal structure of the bacterial RNase III/RNA complex suggests that bacterial enzymes identify their substrates via a complex network of interactions where hydrogen bonds play an important role. The dsRBD of bacterial RNase III contacts the ribose 2′-OH while the nuclease domain forms hydrogen bonds with the phosphate backbone (*23*). Consistently, the solution structure of Rnt1p dsRBD in complex with a model substrate revealed six 2′-OH-mediated hydrogen bonds (*15*). Interestingly, four of these interactions are located in the substrate primary binding site formed by the tetraloop and adjacent four base pairs (*19*). However, the functional impact of these hydrogen bonds and their contribution to substrate selection and cleavage remain unclear.

In this study, we investigated the hydrogen bond requirement for substrate recognition by Rnt1p using bipartite substrates that allow the separation of defects in binding and cleavage. Single and multiple substitutions of ribonucleotides with 2′-*O*-methyl ribonucleotides (2′-O-Me) or 2′-fluoro ribonucleotides (2′-F) were performed to identify hydrogen bonds critical for substrate binding and cleavage. The results suggest that while Rnt1p cleavage does not require hydrogen bond mediated interactions near the cleavage site, it interacts with multiple nucleotides near the stem−loop region to determine the substrate identity. The position of critical 2′-OH differs depending on the sequence and structure of the tetraloop. This indicates that the RNase III broad spectrum of substrates is maintained, at least in part, through a flexible network of interactions that adapts to changes in the substrate structure while maintaining the proper position of the nuclease domain relative to the cleavage site.

MATERIALS AND METHODS

Strains and Plasmids. Yeast strains used in Figure 2 were grown and manipulated using standard procedures (*24, 25*). The strain YHM111-U2L2 was generated by transforming the YHM111 strain (*MATa, trp1, ura3-52, ade2-101, his3, lys2, snr20*::LYS2) (*26*) with the pRS314/U2Δ*S* tem/L2 construct as previously described (*27*).

In Vitro Enzymatic Assays. Recombinant Rnt1p and ΔN-term were produced in bacteria and FLPC purified as described (*28*). RNA transcripts were generated by T7 RNA polymerase and gel purified as described previously (*18*). Chemically synthesized RNA oligoribonucleotides were purchased from Integrated DNA Technologies (Coralville, IA) or University Core DNA Services (Calgary, Alberta, Canada). RNA fragments were 5′-end-labeled using [γ-^{32}P]ATP as previously described (*19*). Reconstitution of *in trans* substrates was obtained by mixing equimolar amounts of different guides (the sequences are indicated in each figure) and target RNAs (TL; 5′-GAUAAAGCUAAU-GUUUUGGAAUCUUCAAGAUUAUGGAG-3′), and 3 fmol of 5′-end-labeled target RNA was added as a tracer to track multiple turnover reactions. Full time courses were performed for all substrates with the exception of those in Figures 4 and 5 where selected time points chosen based on the reciprocal full time course of the unmodified substrate were examined. For single turnover conditions, 6 pmol of guide RNA was mixed with 3 fmol of 5′-end-labeled target RNA. Cleavage reactions were performed by incubating 30−60 nM Rnt1p with the different substrates for 10 min at 30 °C in 20 μL of reaction buffer (30 mM Tris-HCl (pH 7.5), 5 mM spermidine, 0.1 mM DTT, 0.1 mM EDTA (pH 7.5), 10 mM $MgCl_2$) supplemented with 150 mM KCl (Figures 1 and 3) or 75 mM KCl (in Figures 4 and 5). Changing the monovalent salt concentration in Figures 4 and 5 was necessary to allow a direct comparison between Rnt1p and the salt-sensitive ΔN-term version (*13*). Cleavage products were separated on 20% denaturing PAGE and quantified as described (*18*). Size markers were generated by alkaline hydrolysis of 5′-end-labeled target RNA. Calculations were performed using GraphPad Prism 4.03 software (GraphPad Software, CA). All experiments were repeated at least three times.

Electrophoretic Mobility Shift Assay (EMSA). Protein binding experiments were performed as previously described (*17*) with 3 fmol of 5′-end-labeled RNA. For bipartite substrates, 3 fmol of 5′-end-labeled guide RNA was incubated with 2 pmols of unlabeled target RNA prior to the incubation with Rnt1p. The protein concentrations used in the assays ranged from 0.5 to 9 μM. Bands were quantified using an Instant Imager with associated software (Packard, Meriden, CT), and calculations were performed using GraphPad Prism 4.03 software (GraphPad Software, CA). All experiments were performed at least three times. A typical EMSA result is presented in Supporting Information Figure 2.

RNA Electroporation in Yeast Living Cells. Preparation of electrocompetent cells and electroporation were performed essentially as previously described (*27*) with minor modifications. Briefly, YHM111-U2L2 yeast cells were grown at 30 °C in 500 mL of YC-Trp and harvested in late log phase. Electrocompetent cells were obtained with successive washes of the cell pellet with ice-cold 1 M sorbitol. The final pellet was resuspended in 500 μL of ice-cold 1 M sorbitol, and 40 μL of this suspension was used per electroporation. For each transformation, 2 nmol of guide RNA was used. The pulse was performed at 1.5 kV, 25 μF, and 200 Ω with the Bio-Rad MicroPulser (Bio-Rad, Richmond, CA). Immediately after the pulse, cells were diluted with 1 mL of ice-cold 1 M sorbitol and transferred into a tube containing 4 mL of YC-trp media containing 12.5 μg of thiolutine/mL to stop *de novo* transcription. After 20 min incubation at 30 °C, cells were harvested and total RNA was extracted.

Primer Extension. Primer extension analysis was performed essentially as described before (*27*). Briefly, 5 μg of total RNA was incubated with 1 ng of 5′-end-labeled primer (5′-GAGTATGCCGCCAATTAGTG-3′) for 2 min at 65 °C followed by 30 min incubation at 37 °C. After addition of the reaction mixture, samples were incubated for 40 min at 42 °C. Reactions were stopped by addition of EDTA and

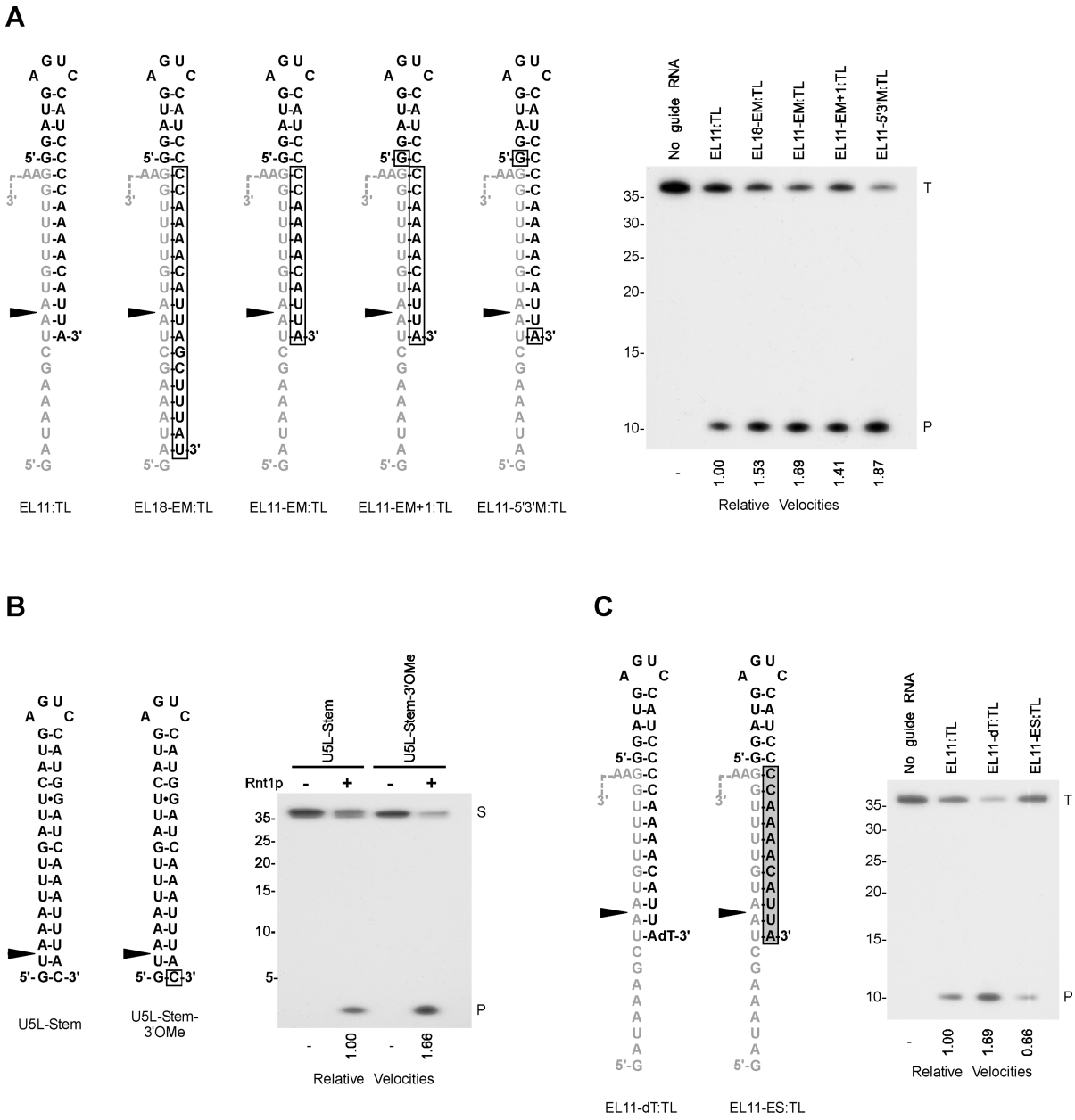

FIGURE 1: Rnt1p cleavage of substrates with chemically modified stems. (A) Rnt1p binding and cleavage do not require 2′-hydroxyl groups opposite of the cleavage site. Guide RNAs containing 2′-*O*-methyl ribonucleotides (boxed regions) were annealed to 5′-end-labeled target RNA (TL, shown in gray) and tested for cleavage with recombinant Rnt1p. (B) The introduction of 2′-O-Me enhances Rnt1p cleavage independent of substrate sequence and structure. A standard substrate formed *in cis* derived from the U5 snRNA 3′-end (*30*) and its 2′-O-Me modified version were tested for cleavage in the absence (−) or presence (+) of Rnt1p. (C) Introduction of phosphorothioate, but not an inverted deoxythymidine, inhibits *in vitro* cleavage by Rnt1p. A mix of target (TL) and guide RNAs containing an inverted deoxythymidine at its 3′-end (EL11-dT) or containing phosphorothioate-bonded ribonucleotides (EL11-ES, gray box) were tested for cleavage by Rnt1p. In each assay, substrate/protein ratio of 30:1 was incubated for 10 min at 30 °C under physiological salt concentration (150 mM KCl). Uncleaved substrates (T or S) and cleavage products (P) were separated by denaturing PAGE, and the bands were quantified. Cleavage rates relative to the nonmodified substrate were calculated from at least three independent experiments, and the average values are indicated below the gels with a maximum standard deviation of the mean of ± 0.10. The position of the RNA ladder is shown on the left. Arrowhead indicates the observed cleavage site. The dashed line symbolizes an extension of 17 ribonucleotides at the 3′-end of TL.

successive treatments with RNase A and proteinase K. The extended products were separated on a 6% denaturing PAGE and visualized by autoradiography. The same primer was used for the sequencing reactions performed using T7 sequencing kit from USB (USB Corp., Cleveland, OH).

RESULTS

The Presence of Phosphate and Not 2′-Hydroxyl Group near the Cleavage Site Is Required for Cleavage by Rnt1p. Earlier studies have shown that the replacement of ribonucleotides 5′ to the scissile bond with deoxyribonucleotides or 2′-*O*-methyl ribonucleotides reduces, but does not inhibit, cleavage by Rnt1p, indicating that the 2′-OH group adjacent to the scissile bond is not directly involved in the cleavage chemistry (*29*). In contrast, multiple deoxyribonucleotide substitutions at the 3′-end of the G2 tetraloop, which do not alter the cleavage site, reduced binding and prevented cleavage by Rnt1p (*29*). The interpretation of these results is difficult because it is not clear whether they arise from

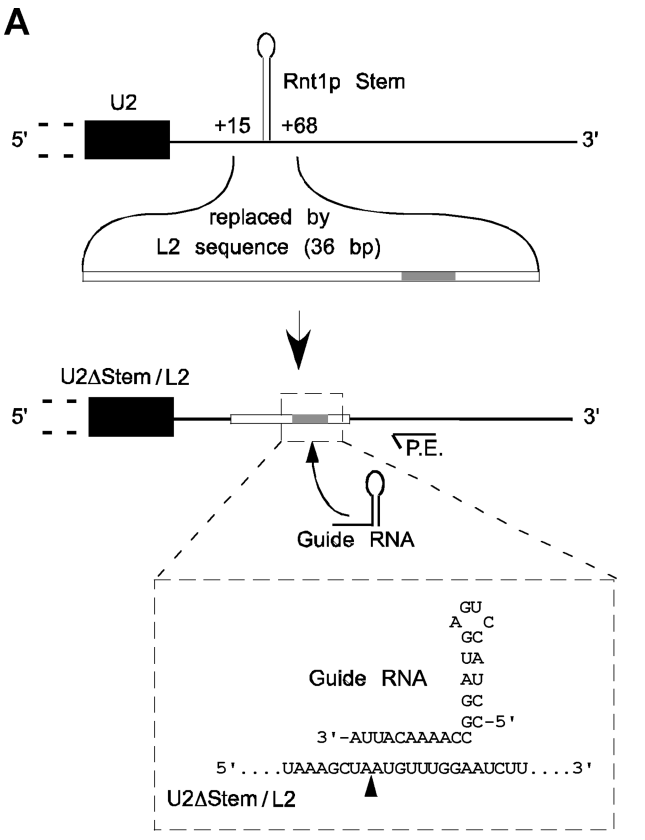

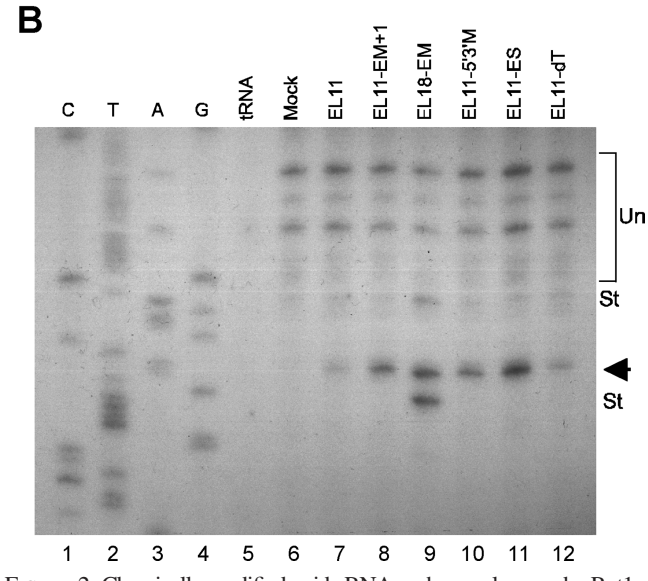

FIGURE 2: Chemically modified guide RNAs enhance cleavage by Rnt1p *in vivo*. (A) Schematic representation of the U2 3′-end flanking region in which the canonical Rnt1p processing signal was replaced with a 36 bp fragment (L2) containing a sequence complementary to the 3′ extension of the guide RNAs (in gray). The position of the oligonucleotide used for primer extension (P.E.) is indicated. (B) Modified guide RNAs direct precise cleavage of U2 3′-end *in vivo*. Total RNA was extracted from yeast cells electroporated with water (Mock) as a negative control or with the different guide RNAs described in Figure 1. The cleavage site was mapped by reverse transcription using the 5′-end-labeled primer (P.E.) shown in (A). tRNA was used as template in the reverse transcription reaction to ensure probe specificity. The primer extension products were separated on 6% denaturing PAGE and compared to DNA sequence produced by the same primer. The arrowhead indicates the position of the guide-dependent cleavage site. Unspecific (Un) and secondary (St) products caused by cleavage-independent polymerase arrest are indicated on the right.

failure to form critical hydrogen bonds, sugar-dependent changes in structure, or intolerance to mixed DNA/RNA helix (*29*). In order to better define the chemical requirement for substrate recognition and the position of 2′-OH critical for interaction with Rnt1p, we introduced single or multiple ribonucleotide modifications and followed their impact on the binding and cleavage of a bipartite substrate that allows the separation of binding and cleavage events. This recently developed bipartite substrate (EL11:TL) (*27*) is based on the sequence of Rnt1p cleavage signal found near the 3′-end of U5 snRNA (*30*). As shown in Figure 1A, EL11:TL is formed by annealing two complementary RNA fragments: the first acts as a guide and contains Rnt1p binding site (e.g., G2 tetraloop) and the other acts as a cleavable target. As expected, cleavage of the bipartite substrate (EL11:TL) obeys the kinetics of natural RNA substrates (*27*) (Supporting Information Figure 1) and allows cleavage in a single site within the target sequence (Figure 1A and Table 1). Surprisingly, replacement of all ribonucleotides below the fifth position from 3′-end of the G2 tetraloop with 2′-O-Me (EL18-EM:TL and EL11-EM:TL) did not inhibit but instead enhanced the cleavage of the target sequence (Figure 1A). Introduction of additional 2′-*O*-methyl group at the 5′-nucleotide of the guide sequence (EL11-EM+1:TL) did not have additional effects on cleavage. On the other hand, modification of ribonucleotides at both ends of the guide sequence (EL11-5′3′M:TL) increased cleavage (Figure 1A) and turnover rate by 5 times when compared to the unmodified substrate (Table 1). This increase in the k_{cat} value led to considerable increase in cleavage efficiency, suggesting that the inclusion of 2′-*O*-methyl group at the 3′-end of the guide sequence accelerates catalysis.

We next tested the effect of modifying the 3′-terminal ribonucleotide on the cleavage of conventional *in cis* substrates. As shown in Figure 1B, a single nucleotide modification at the 3′-end of a model substrate found at U5 snRNA 3′-end (U5L-stem-3′OMe) was sufficient to increase cleavage by 60% when compared to unmodified RNA (U5L-stem). Therefore, this increase in cleavage is not specific to the stem sequence or to the 2′-*O*-methyl moiety since it could also be achieved by other modifications like addition of an inverted deoxythymidine (dT) (EL11-dT:TL) (Figure 1C). Introduction of a phosphorothioate linkage in the strand opposing the cleavage site (EL11-ES:TL) enhanced binding in the absence of Mg^{2+} (Table 1), while strongly inhibiting cleavage (Figure 1C) and reducing both k_{cat} and K'_M without affecting the catalytic efficiency (k_{cat}/K'_M). This situation is characteristic of an unproductive binding of the enzyme to its substrate. This suggests that the phosphate backbone does not play an important role in the formation of the stable RNA/protein complex provided by the dsRBD but instead is required for the formation of the nuclease domain dependent catalytic complex. Alternatively, the observed reduction in the cleavage efficiency may be explained at least in part by the fact that phosphorothioates are not stereospecific. In theory, the modified substrate EL11-ES:TL may form 2^{11} different isomers (2 isomers for each 11 phosphorothioate linkages) with variable reactivities (*31–33*). We conclude that Rnt1p does not require the presence of 2′-OH groups of the ribonucleotides opposing the cleavage site.

In order to test the effect of nucleotide modifications on Rnt1p cleavage *in vivo,* we transformed different guide

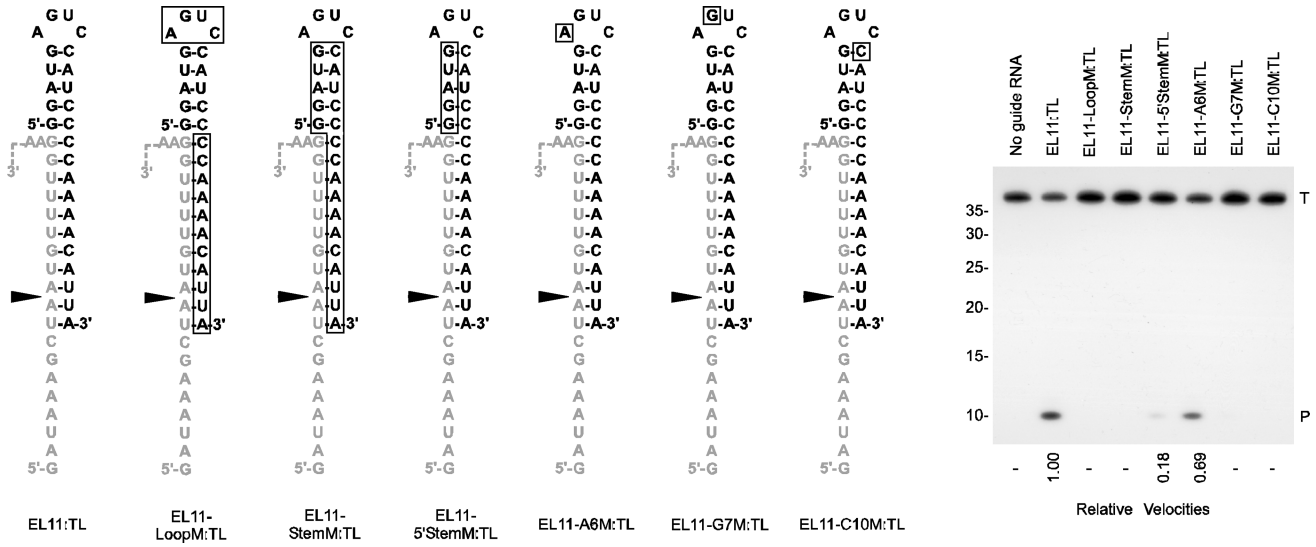

FIGURE 3: Introduction of 2′-O-Me in Rnt1p primary binding site inhibits both binding and cleavage. Bipartite substrates containing 2′-*O*-methyl ribonucleotides (boxed regions) were tested for cleavage by recombinant Rnt1p. *In vitro* cleavage reactions were performed essentially as described in Figure 1 with the exception that single turnover conditions were used. The dashed line indicates 17 ribonucleotide extension at the target 3′-end, and the arrowhead indicates the position of the cleavage site. The positions of substrates (T) and cleavage products (P) are indicated on the right, while the position of the RNA ladder is on the left. Cleavage rates relative to the nonmodified substrate were calculated from three independent experiments, and average values are indicated at the bottom with a maximum standard deviation of the mean of ±0.10.

RNAs (used in Figure 1) into yeast strains expressing a previously established U2 snRNA reporter gene (*27*) that carries at its 3′-end a sequence complementary to the guide RNAs (Figure 2A). The cleavage product generated at U2 snRNA 3′-end was detected by reverse transcription using a primer complementary to the sequence downstream of the target cleavage site. As shown in Figure 2B, no cleavage products were detected when tRNA (lane 5) was used as a template or in RNA extracted from mock-transformed cells (lane 6). Bands arising from premature stops of the primer extension (Un) were observed with all RNAs including those extracted from mock-transfected cells. In contrast, weak guide-dependent cleavage products were observed upon the transformation of either unmodified RNA (lane 7) or guide RNA carrying an inverted dT (lane 12). As predicted, strong cleavage was detected upon transformation of the different 2′-O-Me-modified guide RNAs (lanes 8−10). In the case of EL18-EM, bands corresponding to guide-dependent but cleavage-independent stop in primer extension (St) were observed (lane 9 and data not shown). Surprisingly, transformation of EL11-ES (lane 11), which contains phosphorothioate linkages, produced strong cleavage *in vivo* when compared to unmodified RNA. This could be probably explained by the increase in the stability of EL11-ES in cell extracts when compared with that of the unmodified EL11 (data not shown), which may compensate for the poor reactivity of EL11-ES *in vitro*. It is also possible that the effect of the phosphorothioate linkage is offset *in vivo* by cellular factors which can either favor the formation of catalytically competent RNA/protein complexes (*34*) or influence the configuration of the substrate's phosphate backbone. Northern blot analysis using probes specific to the sequence of U2 snRNA confirmed the results obtained by primer extension and indicated that EL18-EM and EL11-5′3′M are the most effective guide RNAs *in vivo* (data not shown). The results confirm Rnt1p's tolerance for the presence of 2′-*O*-methyl ribonucleotide opposing the cleavage site and suggest that in yeast, as in mammalian cells (*35*), 2′-*O*-methyl-modified oligonucleotides are good tools for gene silencing.

Introduction of 2′-O-Methyl Groups within the G2 Tetraloop Inhibits Binding and Cleavage. The solution structure of Rnt1p dsRBD in complex with a model RNA substrate identified 2′-OH-dependent protein contacts with four variable nucleotides near the conserved G2 tetraloop. In contrast, no hydrogen bond interactions were identified with the highly conserved essential guanosine in position 2 of the tetraloop (*36*). In order to evaluate the importance of the 2′-hydroxyl moiety for substrate recognition, we introduced single and multiple 2′-O-Me near the G2 tetraloop and measured the impact on Rnt1p binding and cleavage. 2′-O-Me substitutions of all four nucleotides in the tetraloop (EL11-loopM:TL) inhibited binding and cleavage (Figure 3 and Table 1), indicating that the ribose 2′-OH moieties in the tetraloop are important for both activities. Modification of the 5 bp below the tetraloop (EL11-stemM:TL) inhibited both binding and cleavage (Table 1 and Figure 3). Substitutions of the five ribonucleotides of one strand of the dsRNA helix at the 5′-end of the loop (EL11-5′stemM:TL) reduced binding and inhibited cleavage albeit not to the same extent as that observed upon the substitution of both strands of the helix (EL11-stemM:TL). These results demonstrate the importance of the upper stem 2′-OH moieties for Rnt1p binding and cleavage. Substitution of the adenosine in the first position of the loop with 2′-O-Me (EL11-A6M:TL), which does not hydrogen bond with the dsRBD (*15*), reduced both K'_M and k_{cat} but had no effect on catalytic efficiency or binding (Table 1 and Figure 3). Single 2′-O-Me substitution of either the conserved guanosine (EL11-G7M:TL) or the first nucleotide downstream of the loop 3′-end (EL11-C10M:TL) affected binding and prevented cleavage. This strongly suggests that the 2′-OH of these two ribonucleotides supports critical protein/RNA interactions in the context of the full enzyme, which cannot be detected in dsRBD/RNA complex (*15*).

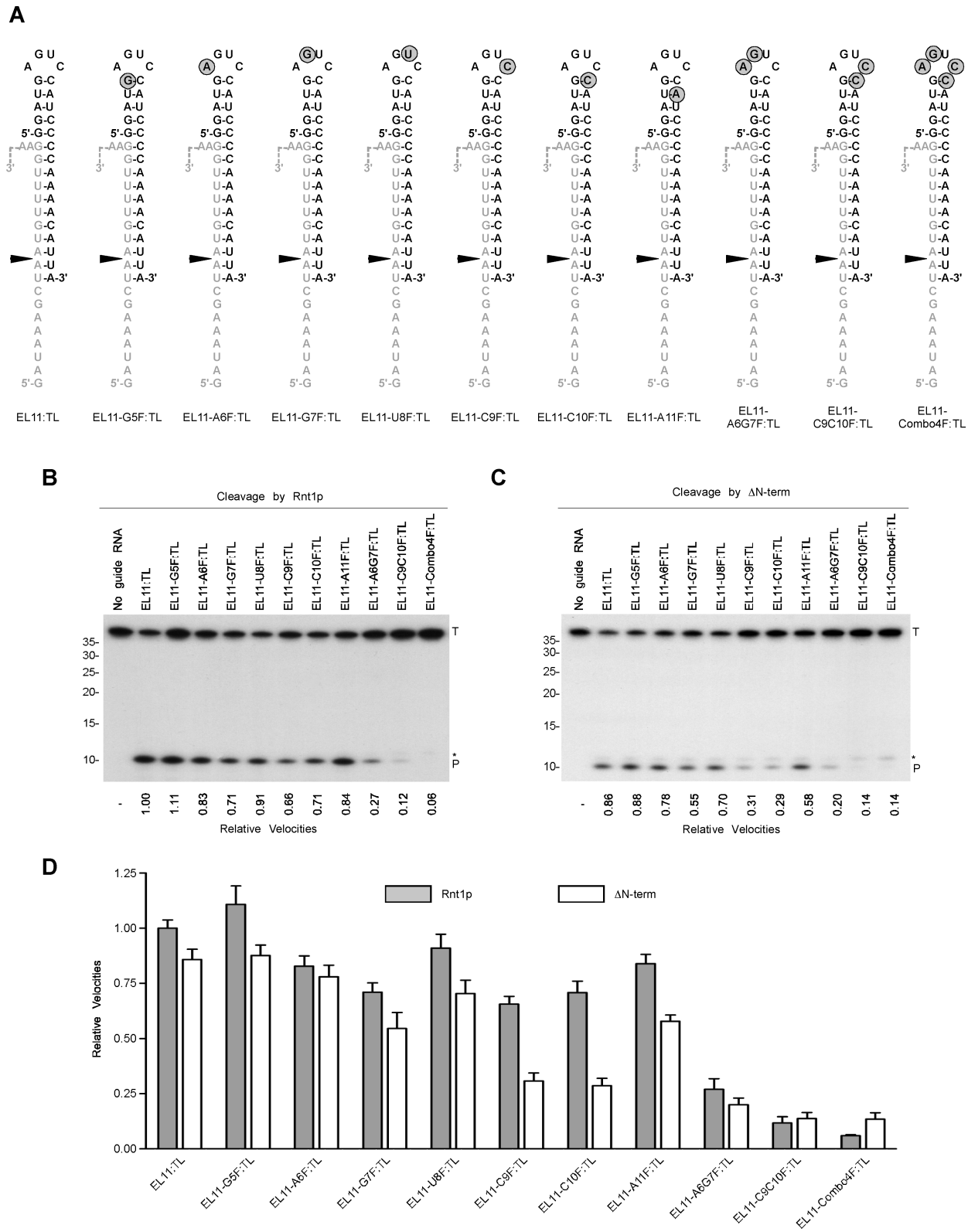

FIGURE 4: Rnt1p cleavage of RNA capped with 2′-F modified G2 tetraloop. (A) Schematic representation of 2′-F (gray circles) modified guide RNAs annealed to their target (TL). The bipartite substrates were tested for cleavage by Rnt1p (in (B)) or by ΔN-term (in (C)), a protein lacking the N-terminal domain of Rnt1p. Cleavage was carried essentially as described in Figure 1 except that the reactions were performed under 75 mM KCl with a substrate/protein ratio of 10:1. Three independent experiments were used to calculate the relative cleavage velocity (shown below the gels). The asterisk indicates the products generated by cleavage at a noncanonical site 13 nucleotides from the tetraloop. This aberrant cleavage product was included in the relative velocity calculation. (D) Graphical comparison of the cleavage rates obtained with different guide RNA modifications shown in (B) and (C). Rnt1p and ΔN-term values are shown in gray and white, respectively. Error bars represent the standard deviation of the mean.

However, we cannot exclude at this stage the possibility that some or even all of the observed effects of the 2′-O-Me substitutions are caused by perturbation of the RNA structure or steric hindrance of Rnt1p binding.

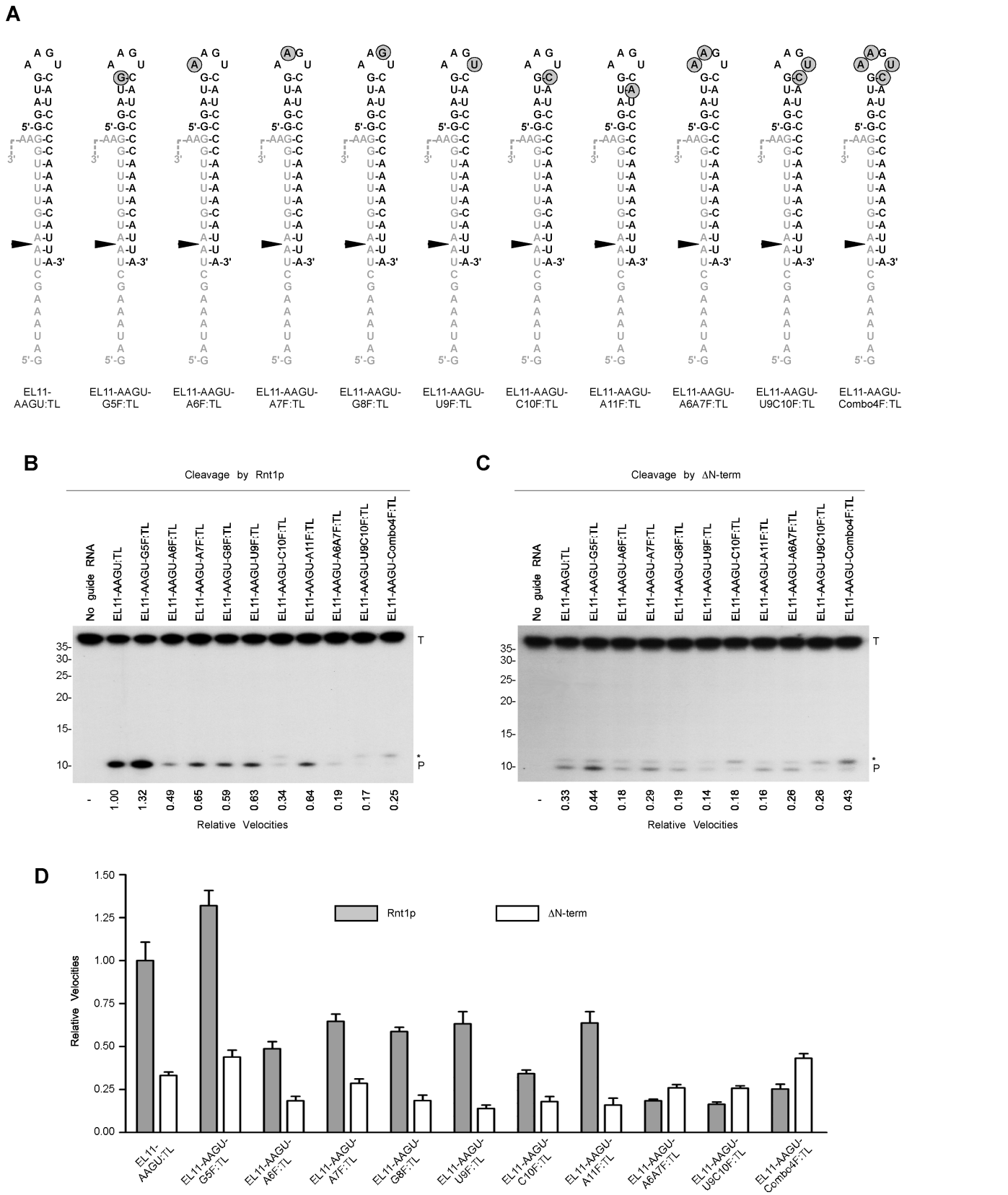

FIGURE 5: Rnt1p cleavage of RNA capped with 2′-F modified A1 tetraloop. (A) Illustration of the 2′-F (gray circles) modified A1 guides annealed to their targets (TL). The different substrates were cleaved by Rnt1p (B) or ΔN-term (C) and the relative cleavage rates calculated and graphically compared (D) as described in Figure 4.

2′-F Substitutions Identify Multiple 2′-OH-Dependent Interactions Required for Substrate Recognition. In order to differentiate between ribonucleotides involved in the formation of hydrogen bonds critical for Rnt1p binding and cleavage from those essential for the formation of the RNA fold recognized by the enzyme, we individually substituted every ribonucleotide in or near the G2 tetraloop with 2′-fluoro ribonucleotide (Figure 4A). The 2′-F modification does not alter the conformation of the native ribonucleotide and thus minimizes the perturbation of the substrate structure.

Table 1: Kinetic Parameters of Rnt1p Cleavage of Bipartite Substrates[a]

substrate	K'_d (μM)	k_{cat} (min^{-1})	K'_M (μM)	k_{cat}/K'_M ($min^{-1}\cdot\mu M^{-1}$)
EL11:TL	2.3 ± 0.2	5.2 ± 0.3	1.7 ± 0.3	3.0 ± 0.6
EL18-EM:TL	1.3 ± 0.1	14.9 ± 0.8	2.4 ± 0.4	6.3 ± 1.0
EL11-EM:TL	4.4 ± 0.3	33.1 ± 2.0	3.2 ± 0.5	10.3 ± 1.7
EL11-EM+1:TL	2.9 ± 0.3	18.1 ± 1.4	1.6 ± 0.4	11.1 ± 2.7
EL11-5′3′M:TL	2.6 ± 0.3	24.0 ± 1.4	1.8 ± 0.3	13.7 ± 2.5
EL11-dT:TL	2.8 ± 0.3	33.1 ± 2.1	3.3 ± 0.5	10.2 ± 1.8
EL11-ES:TL	0.41 ± 0.02	1.7 ± 0.1	0.4 ± 0.1	3.9 ± 1.1
EL11-loopM:TL	>7	n/d	n/d	n/d
EL11-stemM:TL	>7	n/d	n/d	n/d
EL11-5′stemM:TL	5.0 ± 0.5	2.5 ± 0.4	3.6 ± 1.0	0.7 ± 0.2
EL11-A6M:TL	1.7 ± 0.2	1.8 ± 0.2	0.6 ± 0.3	2.8 ± 1.6
EL11-G7M:TL	4.8 ± 0.5	n/d	n/d	n/d
EL11-C10M:TL	>7	n/d	n/d	n/d

[a] The initial rate of cleavage of substrates was measured as a function of substrate concentration. Thirty nanomolar recombinant Rnt1p was incubated with 0.2−12.8 μM bipartite substrates at 30 °C in the presence of 150 mM KCl. The best-fit curves to a Michaelis−Menten scheme were calculated using GraphPad Prism 4.03 software. The apparent dissociation constants (K'_d) were determined by EMSA as described in Materials and Methods. Values are derived from at least three independent experiments, and standard error of the mean was calculated. "n/d" indicates "not determined".

Moreover, the 2′-fluoro moiety exhibits a similar electronegativity pattern and bond polarity as the 2′-hydroxyl (*37*). As shown in Figure 4B,D, introduction of 2′-F in the 5′-end (EL11-G5F:TL) or in the third position (EL11-U8F:TL) of the tetraloop had little negative effect on RNA cleavage. Changes in the first position of the tetraloop (EL11-A6F:TL) or in the second base pair at the 3′-end of the loop (EL11-A11F:TL) reduced RNA cleavage by a modest 15%. The strongest effect (~30%) was observed by the substitution in the second (EL11-G7F:TL) or fourth position (EL11-C9F:TL) of the tetraloop or the closing base pair at the 3′-end of the tetraloop (EL11-C10F:TL). Further analysis of the substitutions that affected the cleavage (EL11-A6F:TL, EL11-G7F:TL, and EL11-C10F:TL) indicated that 2′-F substitutions in the second position of the tetraloop or at the 3′-end closing base pair reduced binding affinity, while substitution in the first position of the loop has no effect on binding (Table 2). On the other hand, all three mutations reduced both K'_M and k_{cat} with little effect on the catalytic efficiency (Table 2). These results indicate that no single 2′-OH in the tetraloop is absolutely essential for the interaction with Rnt1p. They also suggest that substrate recognition is achieved by the formation of a network of hydrogen bonds that involves, at least in part, the ribonucleotides in the second and fourth position of the G2 tetraloop. In order to directly test this hypothesis, we introduced multiple 2′-F substitutions in either position 1 and 2 of the tetraloop (EL11-A6G7F:TL) or position 4 and the first nucleotide of the stem (EL11-C9C10F:TL). As shown in Figure 4, multiple substitutions exerted synergistic inhibitory effect reducing the cleavage efficiency by more than 70% when compared with the unmodified substrate (EL11:TL). As expected, simultaneous substitution of the nucleotides at the 5′-end and 3′-end of the tetraloop (EL11-combo4F:TL) almost completely inhibited the cleavage by Rnt1p. Together, the results suggest that Rnt1p cleavage efficiency is determined, at least in part, by the number of available hydrogen bonds in the upper stem−loop region.

The 2′-OH substitutions confirmed the presence of two of the hydrogen bonds predicted by the solution structure of Rnt1p dsRBD/RNA complex (C9 and A11) and identified two new potential hydrogen bonds (G7 and C10) that influence the cleavage reactions but could not be detected in the solution structure (Figure 4) (*15*). This suggests that the 2′-OH of G7 and C10 influences dsRBD-independent functions of Rnt1p. In order to test this possibility, we examined the impact of 2′-OH substitution on the binding and cleavage of a recombinant version of Rnt1p lacking the N-terminal domain (ΔN-term) (*13*). The N-terminal domain is suggested to influence Rnt1p interaction with the 5′-end of the loop and stabilize the interaction of Rnt1p with its substrate (*13*). Therefore, we expect that substitutions of 2′-OH which contributes to N-terminal domain-dependent functions to have no additional effect on ΔN-term activity, while substitutions acting on other domains should synergistically increase the defects caused by the deletion of Rnt1p N-terminal domain. As expected, deletion of the N-terminal domain did not affect the cleavage of the unmodified EL11:TL under low salt conditions, nor the modified substrates EL11-G5F:TL, EL11-A6F:TL, and EL11-U8F:TL (Figure 4C,D). Modification in the second base pair at the 3′-end of the loop (EL11-A11F:TL) or the conserved guanosine in the second position of the tetraloop (EL11-G7F:TL) modestly reduced the cleavage rate when compared to EL11:TL. Cleavage of EL11-C9F:TL and EL11-C10F:TL, in which the last position of the tetraloop or the first position in the stem below the tetraloop was modified, was strongly inhibited (Figure 4C). The ΔN-term cleavage kinetics of EL11-A6F:TL was very similar to that of the unmodified RNA EL11:TL, while EL11-G7F:TL and EL11-C10F:TL reduced the rate of catalysis and the catalytic efficiency (Table 2) as observed with cleavage performed using the full enzyme. Deletion of the N-terminal domain had little additional effects on the cleavage of substrates carrying multiple 2′-F substitutions. This is probably due to the already severe defects observed with the substrates carrying multiple substitutions. Nevertheless, analysis of the individual nucleotide substitutions indicates that Rnt1p N-terminal domain does not contribute to the enzyme interaction with C9 and C10 but influences, at least partially, 2′-OH-dependent interactions with G7 and A6. This is consistent with previous chemical footprinting and mutational analyses (*18*) suggesting that while the dsRBD is sufficient for binding with the 3′-end of the loop, the interaction of the enzyme with the 5′-end of the loop is influenced by the N-terminal domain. In addition, deletion of the N-terminal domain induced secondary cleavage at a noncanonical site 13 nucleotide from the tetraloop (Figure 4C), suggesting that the N-terminal domain ensures the correct positioning of the enzyme relative to its substrate.

Rnt1p Uses a Functionally Flexible Network of Hydrogen Bonds To Accommodate Changes in the Substrate Features. In addition to the G2 tetraloop substrates, Rnt1p recognizes a class of RNA hairpins capped with AAGU tetraloop (A1 tetraloop), which differs in sequence and structure from the G2 class. Moreover, chemical footprinting experiments suggest that Rnt1p is positioned differently on A1 and G2 tetraloop substrates (*18*). It is not clear whether Rnt1p uses the same group of 2′-OH to identify the two classes of substrates or uses a substrate-specific network of interactions. In order to answer this question, we measured the effect of 2′-F substitutions in guide RNAs that share the sequence of EL11:TL with the exception of the tetraloop, which was

Table 2: Kinetic Parameters of Rnt1p or ΔN-Term Cleavage of 2′-Fluoro-Modified Substrates[a]

	Rnt1p				ΔN-term		
substrate	K'_d (μM)	k_{cat} (min^{-1})	K'_M (μM)	k_{cat}/K'_M ($min^{-1}\cdot\mu M^{-1}$)	k_{cat} (min^{-1})	K'_M (μM)	k_{cat}/K'_M ($min^{-1}\cdot\mu M^{-1}$)
EL11:TL	2.3 ± 0.2	4.2 ± 0.3	2.4 ± 0.3	1.7 ± 0.3	1.1 ± 0.1	0.5 ± 0.1	2.3 ± 0.3
EL11-A6F:TL	2.0 ± 0.1	1.7 ± 0.2	1.1 ± 0.3	1.5 ± 0.4	1.3 ± 0.1	0.7 ± 0.2	1.9 ± 0.6
EL11-G7F:TL	5.8 ± 0.4	1.6 ± 0.2	1.2 ± 0.3	1.4 ± 0.4	0.7 ± 0.1	0.5 ± 0.1	1.3 ± 0.3
EL11-C10F:TL	4.7 ± 0.3	1.0 ± 0.1	1.0 ± 0.2	1.0 ± 0.2	0.7 ± 0.1	1.4 ± 0.3	0.5 ± 0.1
EL11-AAGU:TL	4.7 ± 0.2	1.6 ± 0.1	1.5 ± 0.3	1.1 ± 0.2	0.6 ± 0.1	1.0 ± 0.3	0.6 ± 0.2
EL11-AAGU-A6F:TL	6.6 ± 0.5	0.69 ± 0.04	1.9 ± 0.3	0.4 ± 0.1	0.51 ± 0.04	1.8 ± 0.3	0.3 ± 0.1
EL11-AAGU-A7F:TL	6.2 ± 0.3	0.80 ± 0.04	1.0 ± 0.1	0.8 ± 0.1	0.44 ± 0.04	1.2 ± 0.3	0.4 ± 0.1
EL11-AAGU-C10F:TL	5.0 ± 0.5	0.47 ± 0.04	1.9 ± 0.3	0.25 ± 0.04	0.47 ± 0.04	1.1 ± 0.3	0.4 ± 0.1

[a] The initial rate of cleavage of substrates was measured as a function of substrate concentration. Thirty nanomolar recombinant Rnt1p was incubated with 0.1−6.4 μM bipartite substrates at 30 °C in the presence of 75 mM KCl. Calculations were performed as described in Table 1.

changed from AGUC to AAGU (EL11-AAGU:TL) (Figure 5A). These substrates were evaluated for Rnt1p and ΔN-term binding and cleavage. As shown in Figure 5B,D, the unmodified A1-guide RNA (EL11-AAGU:TL) cleaved the target sequence as efficiently as observed with G2-guide RNA, EL11:TL (Figure 4B,D). However, unlike EL11:TL, the cleavage of EL11-AAGU:TL by the ΔN-term was significantly reduced (Figure 5C,D) indicating that A1 substrates are more dependent on the N-terminal domain than G2 substrates as previously suggested (*18*). Modification of the ribonucleotide at the 5′-end of the closing base pairs (EL11-AAGU-G5F:TL) did not negatively affect Rnt1p or ΔN-term cleavage. All other modifications reduced the relative cleavage rate of Rnt1p by more than 30% with the most striking effect obtained by the modification of the nucleotide below the 3′-end of the tetraloop (EL11-AAGU-C10F:TL). This result is consistent with a cooperative binding mode of A1 substrates in which more nucleotides contribute to substrate recognition than observed in the case of G2 substrates (*18*). Interestingly, the modification of C10 also reduced the cleavage specificity resulting in a strong cleavage at a secondary site closer to the loop underscoring the contribution of this nucleotide for the positioning of the enzyme on its substrate. Multiple 2′-F substitutions (EL11-AAGU-A6A7F:TL, EL11-AAGU-U9C10F:TL, and EL11-AAGU-combo4F:TL) exerted additive inhibitory effects, preventing cleavage at the canonical cleavage site, while enhancing the cleavage at an alternative site closer to the tetraloop (Figure 5). Additional reduction in the cleavage rate by the ΔN-term was observed with all substrates carrying single nucleotide modifications with the exception of EL11-AAGU-G5F:TL and EL11-AAGU-A7F:TL (Figure 5C,D). Deletion of the N-terminal domain did not affect the cleavage of EL11-AAGU-A6A7F:TL, EL11-AAGU-U9C10F:TL, or EL11-AAGU-combo4F:TL but instead enhanced the cleavage at the alternative cleavage site observed upon the modifications of the A1 tetraloop (Figure 5). Unlike their G2 counterparts, the substitution of either the first or the second position of the tetraloop reduced enzyme binding, lowered the rate of catalysis, and decreased the catalytic efficiency (Table 2). Modification of the 3′-end nucleotide of the tetraloop closing base pair did not affect Rnt1p binding or K'_M but reduced the rate of catalysis and catalytic efficiency. In general, while all tested modifications in the G2 tetraloop reduced both K'_M and k_{cat}, the modifications in the A1 substrate reduced the k_{cat} without affecting the K'_M exposing the differences in the role played by the 2′-hydroxyl groups of these tetraloops for Rnt1p cleavage. We conclude that Rnt1p uses different patterns of 2′-OH-dependent interactions for the recognition of A1 and G2 tetraloops.

DISCUSSION

In this study we have shown that Rnt1p, the yeast orthologue of the bacterial RNase III, does not require 2′-hydroxyl groups near the cleavage site but instead requires the presence of the RNA backbone phosphates opposing the cleavage site. This indicates that the formation of the catalytic core requires, at least in part, interaction with the phosphate backbone explaining the broad specificity of the nuclease domain. Indeed, the structure of *Aquifex aeolicus* RNase III/RNA complex revealed that the nuclease domain RNA binding motif (RBM) 3, which is conserved in Rnt1p, forms a hydrogen bond with the nonbridging phosphate oxygen (*23*). In addition, crystal structures of the bacterial RNase III revealed that the nucleophilic attack occurs through coordination of metal ions and water molecules with the phosphate at the scissile bond (*38*). The ribose 2′-OH groups do not seem to have a major contribution in the phosphoryl transfer reaction (*38*). In contrast, the enzyme requires the presence of multiple 2′-OH groups within the substrate binding site (upper stem and tetraloop) for cleavage. The location and number of required 2′-OH differ depending on the sequence and structure of the substrate tetraloop, suggesting that a flexible interaction network allows the enzyme to recognize different tetraloop folds (e.g., both A1 and G2 substrates). Together, the data suggest that Rnt1p may form two different RNA/protein complexes: the first is a magnesium-independent nonproductive complex that forms through 2′-OH-dependent interactions between the dsRBD and the upper stem−loop, while the second complex leads to cleavage and involves the formation of phosphate-dependent interactions with the nuclease domain.

Rnt1p Requires Different Chemical and Structural Features for Substrate Binding and Cleavage. Like bacterial RNase III (*39*), Rnt1p can form a stable complex with RNA in the absence of Mg^{2+} (*13*) and binds small RNA hairpins shorter than 11 bp (*20*). In addition, mutations in the protein or the RNA substrate that decrease binding affinity in the absence of Mg^{2+} do not always lead to cleavage inhibition, and several mutations that prevent catalysis do not inhibit binding (*17*). This suggests that Rnt1p may form two different complexes with different substrate requirements. The first is a nonproductive complex that requires recognition by the dsRBD and forms independently of Mg^{2+}. The second is Mg^{2+}-dependent and requires interaction with both the dsRBD and the nuclease domain and leads to cleavage (*17*).

Consistently, we have found that 2′-O-Me substitution of ribose 2′-OH in the strand opposing the cleavage site increases the rate of catalysis (k_{cat}) by up to 5 times with little effect on the Mg^{2+}-independent substrate affinity (K'_d) and without obligatory change in the apparent Michaelis constant (K'_M) in the presence of Mg^{2+} (Table 1). Evidence for the presence of nonproductive binding during the cleavage reaction could also be deduced from the fact that several individual 2′-fluoro modifications of ribonucleotides forming the primary binding site (upper stem−loop) decreased both k_{cat} and K'_M without impact on the catalytic efficiency (Table 2). Once again, no strict correlation between 2′-OH substitutions that reduce the K'_M and those that increase the K'_d could be observed, suggesting that the complex formed under noncatalytic conditions and the one forming prior to catalysis use different substrate requirements. Indeed, crystal structure of bacterial RNase III carrying mutation in the catalytic domain revealed that the dsRBD domain could independently bind to RNA outside the nuclease domain (*23*). It was also demonstrated that Mg^{2+} is required to induce the conformational change required for the positioning of the RNA duplex within the catalytic valley (*23*), stabilization of the catalytic assembly, and product release (*38*). Therefore, we conclude that binding and cleavage of RNA duplexes by Rnt1p, like other RNase IIIs, are achieved through several transitional steps requiring different chemical interactions and structural conformation. Formation of productive or nonproductive complexes, as well as transition between them, likely depends on the substrate's ability to fulfill these requirements.

Distinguishing between Structural and Chemical Requirements for Rnt1p Substrate Reactivity. To date, most studies of protein/RNA interactions used sugar substitutions such as 2′-deoxy, 2′-deoxy-2′-fluoro-β-D-arabinonucleosides (2′F-ANA), or 2′-*O*-methyl to identify hydrogen bonds required for RNA identification. Unfortunately, these types of substitutions often disturb local structure (*40*) and hinder protein interaction (*41*), which makes the identification of hydrogen bonds critical for substrate selection very difficult. Substitutions with 2′-fluoro ribonucleotides, which preserve the RNA structure and cause minimum disturbance of hydrogen bonds independent protein interaction, are a good alternative for evaluating the role of the tetraloop ribonucleotides in Rnt1p binding and cleavage. Organic fluorine can act as a weak hydrogen bond acceptor under certain conditions that optimize bond formation (*42*). However, the strength of fluorine-based interactions and their functional relevance to enzyme activity remain unclear and largely depend on the strength of the donor group, neighboring atoms, and distance between partners (*42*). In most cases, fluorine-substituted ligands exhibit lower binding affinity and enzymatic activity when the hydrogen bond formation is a prerequisite for enzyme binding and catalysis (*43*). Thus, fluorine substitutions are excellent for probing hydrogen bond requirements especially those believed to be essential for Rnt1p binding and cleavage as those examined in this study. For example, fluorine substitution is particularly suitable for examining the contribution of the 2′-OH of the highly conserved guanosine present in the second position of the G2 tetraloop to binding and cleavage. Substituting this guanosine with another ribonucleotide (*19*), with deoxyguanosine (*29*), or with 2′-*O*-methylguanosine (Figure 3) strongly reduced Rnt1p binding and inhibited cleavage despite the fact that no interactions were detected between this nucleotide and the dsRBD by NMR (*15*). This led to the conclusion that the conserved G is only important for the tetraloop fold recognized by Rnt1p (*20*) and does not contribute biochemically to substrate recognition. By substituting this nucleotide with 2′-fluoroguanosine, we were able to reveal that the 2′-hydroxyl group of this nucleotide is equally important for substrate cleavage as the nucleotide at the fourth position of the tetraloop (Figure 6A), which was shown to hydrogen bond with the dsRBD in the solution structure of Rnt1p dsRBD/RNA complex (*15*). This underscores the advantage of 2′-fluoro modifications as a precise probe for 2′-OH requirements. More importantly, these results clearly show that the conserved G plays a dual role in preserving the G2-substrate structure and in forming direct and specific interaction with the enzyme. In general, the introduction of 2′-O-Me at any position near the enzyme primary binding site was much more inhibitory to binding and cleavage than given 2′-F substitutions (Tables 1 and 2). This indicates that Rnt1p is much more sensitive to changes in the overall structure of the tetraloop than to position-specific hydrogen bonding, which explains Rnt1p's capacity to recognize tetraloops with different sequence composition (*4*).

Identification of Hydrogen Bonds Involved in Substrate Binding and Cleavage. The solution structure of Rnt1p dsRBD in complex with a model G2 substrate indicated that the dsRBD forms a total of six direct or water-mediated hydrogen bonds with 2′-OH groups of the RNA (*15*). Four of those are formed between the upper stem−loop region and helix α1, suggesting that these interactions are critical for binding and perhaps for cleavage (Figure 6A). However, individual substitution of the 2′-OH involved in the formation of these four hydrogen bonds with 2′-F did not inhibit cleavage (Figure 6A). Substitutions that prevent hydrogen bond formation between the 5′-end of the closing base pair and the aspartic acid in position 367 of the dsRBD or between the third position of the tetraloop and arginine in position 372 did not have any negative effect on cleavage of G2 substrates (Figure 4). Together, these results suggest that not all hydrogen bonds formed between the dsRBD and the RNA are essential for cleavage. However, we cannot formally exclude the fact that some minor roles of certain hydrogen bonds observed in the NMR structure were missed because they were maintained by the fluorine substitutions (*42*). On the other hand, it should also be noted that the hydrogen bonds observed in the solution structure between the RNA and the truncated dsRBD (*15*) may not reflect the interactions formed in the context of the full enzyme. Substituting the 2′-OH required for the formation of the hydrogen bond between the fourth nucleotide of the tetraloop and serine 376 moderately reduced cleavage. In addition, weak effect was observed upon the disruption of the hydrogen bond between the second nucleotide below the 3′-end of the tetraloop and lysine 371 (Figure 4).

Interestingly, some cleavage reduction was observed by substituting positions one and two of the tetraloop as well as the first nucleotide below the 3′-end of the tetraloop, which do not interact with the dsRBD in the NMR structure (*15*). This suggests that the dsRBD forms hydrogen bond with these nucleotides only in the context of the full enzyme. Another possibility is that different domains of Rnt1p interact

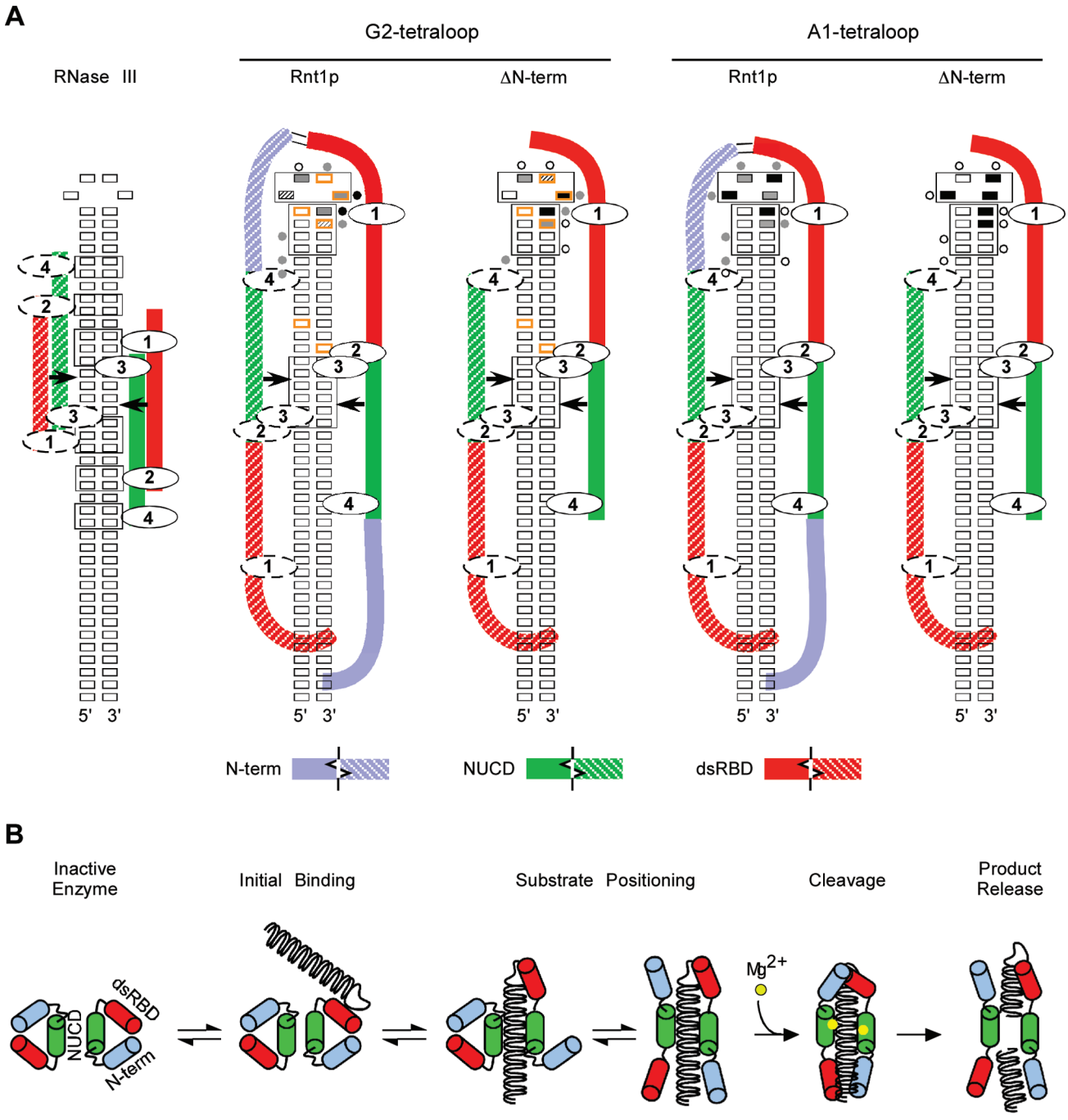

FIGURE 6: Hypothetical model for Rnt1p binding and cleavage. (A) Comparison between bacterial RNase III and Rnt1p mechanisms of substrate recognition. The position of the bacterial RNase III relative to its substrate was based on the cocrystal structure of the RNA protein complex (*23*). Rnt1p nuclease domain position relative to substrate was modeled based on sequence alignment with the bacterial RNase III and location of the cleavage site. The positioning of the dsRBD near the tetraloop was based on the solution structure of Rnt1p dsRBD/RNA complex (*15*), chemical footprinting experiments (*18, 19*), and nucleotide substitution (Figures 4 and 5). Models of G2 and A1 substrates in complex with Rnt1p or with a version of Rnt1p lacking the N-terminal domain (ΔN-term) are shown. The ribonucleotides are represented as rectangles, and the arrows indicate the enzymes cleavage sites. The solid lines represent subunit 1 of the homodimeric enzyme, while hatched lines indicate subunit 2. The dsRNA binding, nuclease, and N-terminal domains are shown in red, green, and blue, respectively. The numbered circles represent the RNA binding motifs (RBMs) of the proteins identified based on the RNA/protein cocrystal structure of bacterial RNase III (*23*) and sequence comparison with Rnt1p. Reactivity epitopes on the substrates that are known to interact with the enzyme or affect its activity are boxed. Nucleotides shown to form hydrogen bonds with Rnt1p dsRBD via their ribose 2′-OH in RNA/dsRBD solution structure are outlined in orange (*15*). Open, gray, and black circles indicate the position of previously observed chemical modifications causing respectively weak, moderate, and strong interference with Rnt1p interaction (*18*). Positions of 2′-F substitutions causing weak, moderate, and strong reductions in cleavage (in Figures 4 and 5) are shown as hatched, gray, and black rectangles, respectively. (B) Proposed mechanism for substrate binding and cleavage by Rnt1p. Like bacterial RNase III (*23*), Rnt1p forms an intermolecular homodimer (*13*) where subunits are likely held together through their nuclease domains. In the case of Rnt1p, intermolecular interaction between the dsRBD and the N-terminal domain was previously demonstrated both biochemically and genetically (*13*). The RNA substrate first interacts with the dsRBD leading to the formation of the catalytic complex in which the binding of the substrate to the nuclease domain triggers conformational changes in both the enzyme and the substrate allowing cleavage.

with these 2′-OH groups. Consistently, positions 1 and 2 of the tetraloop seem to contribute to the function of the N-terminal domain (Figure 4D). These data are consistent with previous mutational analysis, chemical footprinting, and chemical interference that all indicate that the first and second positions interact with the enzyme and play an important role in cleavage (*4, 17*). The significant contribution of the first two nucleotides of G2 tetraloop to RNA cleavage explains in part their high conservation (*4*) and suggests that while Rnt1p may form complexes with a large number of RNA (*18*) and even DNA molecules (*29*), it can only cleave a subset that sponsors the fold of G2 or A1 tetraloops.

A Model for Rnt1p Substrate Identification and Cleavage. Multiple crystal structures of bacterial RNase III/RNA complexes suggest that RNase III first binds its substrate through interactions with the dsRBD that lead, in the presence of Mg^{2+}, to conformational changes in order to form the catalytic core (*23*). The catalytic core is formed through intermolecular homodimerization of the nuclease domains that fit the RNA substrate. In the catalytic core, the RNA duplex is held in place by a total of four RBMs, which form extensive network of hydrogen bonds with two regions of the substrate surrounding the cleavage site (*23*). In addition, each enzyme subunit contains two other RBMs located in the dsRBD (Figure 6A). Since most RBMs, nuclease signature motif, and secondary structure of catalytic domains are conserved in Rnt1p, we were able to use bacterial RNase III tertiary structure (*23, 44, 45*) as a model to position Rnt1p relative to its substrate based on the results of nucleotide substitution (*29*) (Figures 4 and 5), chemical interference (*18*), and the solution structure of Rnt1p dsRBD/RNA complex (*15*) (Figure 6A). The tertiary structure of Rnt1p NUCD was predicted via sequence alignment with the bacterial enzyme (data not shown; the method used to produce the tertiary model is described in the Supporting Information). In this model, the RBM 1 in the dsRBD interacts with the tetraloop upper stem region and is stabilized in place by intermolecular interaction between the dsRBD and the N-terminal domain (*13*). Rnt1p nuclease domain is positioned against the cleavage site in a similar fashion to that of bacterial RNase III and forms contacts with the phosphate backbone. The positioning of Rnt1p RBMs relative to the RNA was possible due to the natural bend of Rnt1p binding signal (*15, 20*), the slight increase in the size of the C-terminal helix of the NUCD, and the linker region between the dsRBD and the NUCD (data not shown). The natural flexible linker of Rnt1p joined the dsRBD and NUCD without the need for structural modifications of the adjacent helices. The position of RBM 4 was more difficult to ascertain given its poor sequence and functional conservation (*17, 23*). The overall binding patterns of G2 and A1 substrates are very similar with the exception that the network of critical interactions in the A1 tetraloop area appears to be more evenly distributed between the 3′- and 5′-end of the tetraloop (Figure 6A), as previously observed with chemical footprinting experiments (*18*). In Figure 6B, we propose a model for Rnt1p binding and cleavage that explains why 2′-OH substitutions displayed position-dependent effects on Rnt1p activities. In this model, the primary interaction between the RNA and the dsRBD occurs independent of the nuclease domain and regardless of the presence or absence of the cleavage site. This interaction is stable in the absence of Mg^{2+} and is largely responsible for the K'_d value of the substrate. In presence of Mg^{2+}, the RNA will be placed within the catalytic valley if it contains a suitable cleavage site. Bacterial RNase III binds Mg^{2+} in the absence of RNA (*45*) and requires it to bind its substrate (*38*). However, it is unclear at which step the magnesium ions are recruited to catalytic core. The formation of the NUCD/RNA complex is mediated in part by phosphate backbone interactions while the overall stability of the enzyme/RNA complex is stabilized by interactions between the dsRBD and the N-terminal domains (*13, 17–19*). The catalytically poised complex also requires the interaction of the RNA with a set of amino acid residues in the dsRBD. This complex determines the enzyme K'_M and k_{cat}.

The new model of Rnt1p substrate interaction described here illustrates Rnt1p's capacity to form alternative productive and nonproductive RNA complexes and explains the molecular basis for the enzyme's broad substrate specificity. Like RNase III, Rnt1p mechanism of action suggests that binding and cleavage occur in at least two distinct steps requiring nonidentical RNA features (*23, 46*). This reveals the potential capacity of these enzymes to influence RNA stability and function through the formation of cleavage-independent ribonucleoprotein complexes (*47*). In addition, the apparently distinct binding and nuclease domain docking and cleavage steps of RNase III illustrated here and proposed by other studies (*44, 47*) suggest that the enzyme may have evolved from the fusion of a dsRNA binding protein with a primitive endoribonuclease.

ACKNOWLEDGMENT

We thank Bruno Lamontagne for help with techniques and training of M.L. and for critical reading of the manuscript. We are grateful to Pierre Lavigne, Xinhua Ji, and Jean-Pierre Perreault for stimulating discussions and comments on the manuscript.

SUPPORTING INFORMATION AVAILABLE

Figure 1, comparison between enzymatically synthesized and chemically synthesized substrates, Figure 2, typical electrophoretic mobility shift assay result, and methods used to model the tertiary structure of Rnt1p. This material is available free of charge via the Internet at http://pubs.acs.org.

REFERENCES

1. Lamontagne, B., Larose, S., Boulanger, J., and Elela, S. A. (2001) The RNase III family: a conserved structure and expanding functions in eukaryotic dsRNA metabolism. *Curr. Issues Mol. Biol. 3*, 71–78.
2. Ritchie, W., Legendre, M., and Gautheret, D. (2007) RNA stem-loops: to be or not to be cleaved by RNAse III. *RNA 13*, 457–462.
3. Lykke-Andersen, K. (2006) Regulation of gene expression in mouse embryos and its embryonic cells through RNAi. *Mol. Biotechnol. 34*, 271–278.
4. Ghazal, G., Ge, D., Gervais-Bird, J., Gagnon, J., and Abou Elela, S. (2005) Genome-wide prediction and analysis of yeast RNase III-dependent snoRNA processing signals. *Mol. Cell. Biol. 25*, 2981–2994.
5. Regnier, P., and Grunberg-Manago, M. (1990) RNase III cleavages in non-coding leaders of Escherichia coli transcripts control mRNA stability and genetic expression. *Biochimie 72*, 825–834.
6. Saito, K., Ishizuka, A., Siomi, H., and Siomi, M. C. (2005) Processing of pre-microRNAs by the Dicer-1-Loquacious complex in Drosophila cells. *PLoS Biol. 3*, e235.

7. Gatignol, A., Laine, S., and Clerzius, G. (2005) Dual role of TRBP in HIV replication and RNA interference: viral diversion of a cellular pathway or evasion from antiviral immunity? *Retrovirology 2*, 65.
8. Nicholson, A. W. (1999) Function, mechanism and regulation of bacterial ribonucleases. *FEMS Microbiol. Rev. 23*, 371–390.
9. Collins, R. E., and Cheng, X. (2005) Structural domains in RNAi. *FEBS Lett. 579*, 5841–5849.
10. Carmell, M. A., and Hannon, G. J. (2004) RNase III enzymes and the initiation of gene silencing. *Nat. Struct. Mol. Biol. 11*, 214–218.
11. Abou Elela, S., Igel, H., and Ares, M., Jr. (1996) RNase III cleaves eukaryotic preribosomal RNA at a U3 snoRNP-dependent site. *Cell 85*, 115–124.
12. Catala, M., Lamontagne, B., Larose, S., Ghazal, G., and Abou Elela, S. (2004) Cell cycle-dependent nuclear localization of yeast RNase III is required for efficient cell division. *Mol. Biol. Cell 15*, 3015–3030.
13. Lamontagne, B., Tremblay, A., and Abou Elela, S. (2000) The N-terminal domain that distinguishes yeast from bacterial RNase III contains a dimerization signal required for efficient double-stranded RNA cleavage. *Mol. Cell. Biol. 20*, 1104–1115.
14. Leulliot, N., Quevillon-Cheruel, S., Graille, M., Van Tilbeurgh, H., Leeper, T. C., Godin, K. S., Edwards, T. E., Sigurdsson, S. T., Rozenkrants, N., Nagel, R. J., Ares, M., and Varani, G. (2004) A new α-helical extension promotes RNA binding by the dsRBD of Rnt1p RNAse III. *EMBO J. 23*, 2468–2477.
15. Wu, H., Henras, A., Chanfreau, G., and Feigon, J. (2004) Structural basis for recognition of the AGNN tetraloop RNA fold by the double-stranded RNA-binding domain of Rnt1p RNase III. *Proc. Natl. Acad. Sci. U.S.A. 101*, 8307–8312.
16. Zhang, K., and Nicholson, A. W. (1997) Regulation of ribonuclease III processing by double-helical sequence antideterminants. *Proc. Natl. Acad. Sci. U.S.A. 94*, 13437–13441.
17. Lamontagne, B., and Abou Elela, S. (2004) Evaluation of the RNA determinants for bacterial and yeast RNase III binding and cleavage. *J. Biol. Chem. 279*, 2231–2241.
18. Ghazal, G., and Elela, S. A. (2006) Characterization of the reactivity determinants of a novel hairpin substrate of yeast RNase III. *J. Mol. Biol. 363*, 332–344.
19. Lamontagne, B., Ghazal, G., Lebars, I., Yoshizawa, S., Fourmy, D., and Abou Elela, S. (2003) Sequence dependence of substrate recognition and cleavage by yeast RNase III. *J. Mol. Biol. 327*, 985–1000.
20. Lebars, I., Lamontagne, B., Yoshizawa, S., Aboul-Elela, S., and Fourmy, D. (2001) Solution structure of conserved AGNN tetraloops: insights into Rnt1p RNA processing. *EMBO J. 20*, 7250–7258.
21. Staple, D. W., and Butcher, S. E. (2003) Solution structure of the HIV-1 frameshift inducing stem-loop RNA. *Nucleic Acids Res. 31*, 4326–4331.
22. Gaudin, C., Ghazal, G., Yoshizawa, S., Elela, S. A., and Fourmy, D. (2006) Structure of an AAGU tetraloop and its contribution to substrate selection by yeast RNase III. *J. Mol. Biol. 363*, 322–331.
23. Gan, J., Tropea, J. E., Austin, B. P., Court, D. L., Waugh, D. S., and Ji, X. (2006) Structural insight into the mechanism of double-stranded RNA processing by ribonuclease III. *Cell 124*, 355–366.
24. Guthrie, C., and Fink, G. R. (1991) *Guide to Yeast Genetics and Molecular Biology*, Academic Press, San Diego, CA.
25. Rose, M. D., Winston, F., and Hieter, P. (1990) *Methods in Yeast Genetics: A Laboratory Course Manual*, Cold Spring Harbor Press, Cold Spring Harbor, NY.
26. Madhani, H. D., and Guthrie, C. (1992) A novel base-pairing interaction between U2 and U6 snRNAs suggests a mechanism for the catalytic activation of the spliceosome. *Cell 71*, 803–817.
27. Lamontagne, B., and Abou Elela, S. (2007) Short RNA guides cleavage by eukaryotic RNase III. *PLoS ONE 2*, e472.
28. Lamontagne, B., and Abou Elela, S. (2001) Purification and characterization of Saccharomyces cerevisiae Rnt1p nuclease. *Methods Enzymol. 342*, 159–167.
29. Lamontagne, B., Hannoush, R. N., Damha, M. J., and Abou Elela, S. (2004) Molecular requirements for duplex recognition and cleavage by eukaryotic RNase III: discovery of an RNA-dependent DNA cleavage activity of yeast Rnt1p. *J. Mol. Biol. 338*, 401–418.
30. Chanfreau, G., Abou Elela, S., Ares, M., Jr., and Guthrie, C. (1997) Alternative 3′-end processing of U5 snRNA by RNase III. *Genes Dev. 11*, 2741–2751.
31. Burgers, P. M., and Eckstein, F. (1979) Diastereomers of 5′-O-adenosyl 3′-O-uridyl phosphorothioate: chemical synthesis and enzymatic properties. *Biochemistry 18*, 592–596.
32. Burgers, P. M., Sathyanarayana, B. K., Saenger, W., and Eckstein, F. (1979) Crystal and molecular structure of adenosine 5′-O-phosphorothioate O-p-nitrophenyl ester (Sp diastereomer). Substrate stereospecificity of snake venom phosphodiesterase. *Eur. J. Biochem. 100*, 585–591.
33. Yamanaka, G., Eckstein, F., and Stryer, L. (1985) Stereochemistry of the guanyl nucleotide binding site of transducin probed by phosphorothioate analogues of GTP and GDP. *Biochemistry 24*, 8094–8101.
34. Giorgi, C., Fatica, A., Nagel, R., and Bozzoni, I. (2001) Release of U18 snoRNA from its host intron requires interaction of Nop1p with the Rnt1p endonuclease. *EMBO J. 20*, 6856–6865.
35. Kraynack, B. A., and Baker, B. F. (2006) Small interfering RNAs containing full 2′-O-methylribonucleotide-modified sense strands display Argonaute2/eIF2C2-dependent activity. *RNA 12*, 163–176.
36. Henras, A. K., Sam, M., Hiley, S. L., Wu, H., Hughes, T. R., Feigon, J., and Chanfreau, G. F. (2005) Biochemical and genomic analysis of substrate recognition by the double-stranded RNA binding domain of yeast RNase III. *RNA 11*, 1225–1237.
37. Egli, M., and Gryaznov, S. M. (2000) Synthetic oligonucleotides as RNA mimetics: 2′-modified RNAs and N3′→P5′ phosphoramidates. *Cell. Mol. Life Sci. 57*, 1440–1456.
38. Gan, J., Shaw, G., Tropea, J. E., Waugh, D. S., Court, D. L., and Ji, X. (2008) A stepwise model for double-stranded RNA processing by ribonuclease III. *Mol. Microbiol. 67*, 143–154.
39. Li, H., and Nicholson, A. W. (1996) Defining the enzyme binding domain of a ribonuclease III processing signal. Ethylation interference and hydroxyl radical footprinting using catalytically inactive RNase III mutants. *EMBO J. 15*, 1421–1433.
40. Ray, A. S., Schinazi, R. F., Murakami, E., Basavapathruni, A., Shi, J., Zorca, S. M., Chu, C. K., and Anderson, K. S. (2003) Probing the mechanistic consequences of 5-fluorine substitution on cytidine nucleotide analogue incorporation by HIV-1 reverse transcriptase. *Antivir. Chem. Chemother. 14*, 115–125.
41. Dertinger, D., Dale, T., and Uhlenbeck, O. C. (2001) Modifying the specificity of an RNA backbone contact. *J. Mol. Biol. 314*, 649–654.
42. Howard, J. A. K., Hoy, V. J., O'Hagan, D., and Smith, G. T. (1996) How good is fluorine as a hydrogen bond acceptor. *Tetrahedron 52*, 12613–12622.
43. Nidetzky, B., Mayr, P., Hadwiger, P., and Stutz, A. E. (1999) Binding energy and specificity in the catalytic mechanism of yeast aldose reductases. *Biochem. J. 344* (Part 1), 101–107.
44. Blaszczyk, J., Gan, J., Tropea, J. E., Court, D. L., Waugh, D. S., and Ji, X. (2004) Noncatalytic assembly of ribonuclease III with double-stranded RNA. *Structure (Cambridge) 12*, 457–466.
45. Blaszczyk, J., Tropea, J. E., Bubunenko, M., Routzahn, K. M., Waugh, D. S., Court, D. L., and Ji, X. (2001) Crystallographic and modeling studies of RNase III suggest a mechanism for double-stranded RNA cleavage. *Structure (Cambridge) 9*, 1225–1236.
46. Sun, W., Jun, E., and Nicholson, A. W. (2001) Intrinsic double-stranded-RNA processing activity of Escherichia coli ribonuclease III lacking the dsRNA-binding domain. *Biochemistry 40*, 14976–14984.
47. Calin-Jageman, I., and Nicholson, A. W. (2003) RNA structure-dependent uncoupling of substrate recognition and cleavage by Escherichia coli ribonuclease III. *Nucleic Acids Res. 31*, 2381–2392.

BI800238U